Polymer 327 (2025) 128417

Contents lists available at ScienceDirect

Polymer

journal homepage: www.elsevier.com/locate/polymer

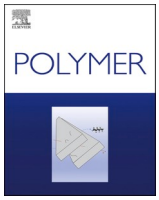

Dimensional and conformational properties of pullulan tris (alkylcarbamate)s in tetrahydrofuran

Yuki Matsumoto [a,b], Shinichi Kitamura [b,c], Rintaro Takahashi [a], Ken Terao [a,*]

[a] Department of Macromolecular Science, Graduate School of Science, The University of Osaka, 1-1 Machikaneyama-cho, Toyonaka, Osaka, 560-0043, Japan
[b] International Polysaccharide Engineering Inc., Center for Research and Development of Bioresources, Osaka Metropolitan University, 1-2, Gakuen-cho, Naka-ku, Sakai, Osaka, 599-8570, Japan
[c] Center for Research and Development of Bioresources, Organization for Research Promotion, Osaka Metropolitan University, 1-2, Gakuen-cho, Naka-ku, Sakai, Osaka, 599-8570, Japan

ARTICLE INFO

Keywords:
Pullulan
Polysaccharide derivatives
Wormlike chain
Chain stiffness
Intramolecular hydrogen bonding

ABSTRACT

Pullulan tris(*n*-butylcarbamate) (PTBC) and pullulan tris(ethylcarbamate) (PTEC) samples with different weight-average molar masses M_w were prepared from pullulan samples with varying chain lengths. Size-exclusion chromatography equipped with multi-angle light scattering detectors (SEC-MALS), small-angle X-ray scattering (SAXS), and viscometry were performed on the samples in tetrahydrofuran (THF) at 25 °C to determine M_w, form factor $P(q)$, radius of gyration R_g, second virial coefficient, and intrinsic viscosity $[\eta]$. Infrared absorption measurements were also conducted to investigate the intramolecular hydrogen bonding between the C═O and NH groups on adjacent monomer units. The obtained $P(q)$, R_g, and $[\eta]$ data were analyzed using the wormlike chain model with excluded volume effects, primarily to determine the contour length per monomer unit and the Kuhn segment length L_K, a measure of chain stiffness. The latter parameter L_K values were found to be 10 nm and 8 nm for PTBC and PTEC, respectively. The resulting chain stiffness was significantly lower than that of the corresponding amylose derivatives. Notably, PTBC and PTEC exhibited few intramolecular hydrogen bonding, in contrast to previously investigated amylose derivatives. This characteristic feature suggests that the free polar groups in pullulan derivatives could offer potential applications as macromolecular recognition materials.

1. Introduction

The global conformation of polymer chains in solution is one of the most important properties because it is related to the viscosity and viscoelastic properties of polymer solutions as well as the solubility of polymers. The relationship between the global conformation and the chemical structure of polymers has therefore been widely investigated in terms of the rotational isomeric state (RIS) model [1,2]. This method has been successful for flexible polymers in organic solvent systems [3], while polymer-solvent interactions can cause significant changes in polymer dimensions. On the other hand, it is not easy to predict the polymer dimensions when the polymer backbone has a semiflexible or rigid nature, because the weak bending as well as some specific conformations such as kinks can influence the global conformation of the polymer chain. In this case, the wormlike chain [4], or more generally, the helical wormlike chain [5], is a good model to describe and characterize the polymer chains.

Polysaccharides and their derivatives are good model polymers because, unlike vinyl polymers, the repeat unit is perfectly uniform. An example is the polyglucans, which show significantly different solubilities between cellulose (β-1,4-glucan), amylose (α-1,4-glucan), curdlan (β-1,3-glucan), dextran (α-1,6-glucan), and pullulan (α-1,4-; α-1,6-glucan). Among these polysaccharides, only dextran and pullulan are soluble in water over a wide molar mass range. Historically, phenylcarbamate derivatives of polysaccharides have been well investigated [6–22] to determine molar mass as well as dimensional properties in solution due to their high solubility in common organic solvents and almost no chain scission during preparation. Because the polar groups tend to form intramolecular hydrogen bonding [23,24], cellulose and amylose phenylcarbamates are known to have relatively high chain stiffness [6,19,24]. Later, carbamate derivatives of polysaccharides were found to be useful as chiral stationary phases for chiral HPLC [25–29].

* Corresponding author.
E-mail address: terao.ken.sci@osaka-u.ac.jp (K. Terao).

https://doi.org/10.1016/j.polymer.2025.128417
Received 16 February 2025; Received in revised form 13 April 2025; Accepted 15 April 2025
Available online 16 April 2025

This may be related to the high chain stiffness and regular helical structure of polysaccharide derivatives, as deduced from the comparison of chiral separation ability with nonlinear polysaccharide derivatives [30–35].

Amylose and cellulose alkylcarbamates are well soluble in various organic solvents [36]. Recently, we demonstrated the relationship between local helical structures and chain stiffness for alkylcarbamates of amylose [37–40] and cellulose [41] in organic solvents. In particular, the rigid helical structure of the amylose alkylcarbamates with short side chains was found to be stabilized by the intramolecular hydrogen bonding [36,42] while the cellulose carbamates have less hydrogen bonding and lower chain stiffness than those of the amylose derivatives [41]. If this difference is due not only to hydrogen bonding between adjacent glycosidic groups but also to the continuous helical structure of α-1,4-glucan, pullulan alkylcarbamate may have different local conformational features compared to amylose alkylcarbamates. In this regard, although pullulan has a much higher solubility than amylose and cellulose, especially in water, we found in our preliminary investigation that pullulan octadecylcarbamate was much less soluble in common organic solvents than the former two polysaccharide derivatives. Consequently, we investigated the dimensional, hydrodynamic, and spectroscopic properties of samples of pullulan alkylcarbamates, whose chemical structure is shown in Fig. 1, in tetrahydrofuran (THF). The resulting data were analyzed in terms of the wormlike chain to reveal the relationship between conformational features and intermolecular interactions in the solvent.

2. Experimental section

2.1. Preparation of PTBC and PTEC samples

Pullulan tris(alkylcarbamate) samples were synthesized in the manner previously reported for amylose alkylcarbamate derivatives [37]. A commercially available pullulan sample (Nagase Viita Co., Japan) was selected for this study. Fractional precipitation was performed on the sample to obtain different molar mass samples with weight-average molar mass M_w ranging from 60 to 900 kg mol^{-1}. A typical procedure for the synthesis of a pullulan tris(*n*-butylcarbamate) (PTBC) sample is described as follows.

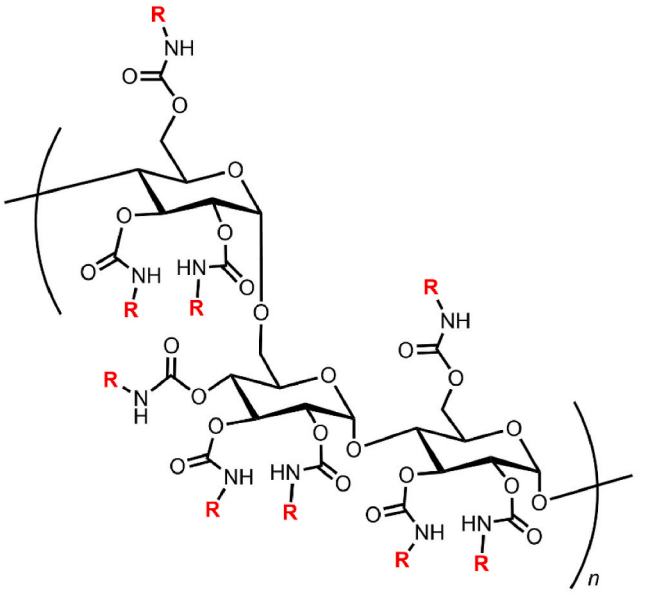

Fig. 1. Chemical structures of pullulan tris(ethylcarbamate) (PTEC), pullulan tris(*n*-butylcarbamate) (PTBC), and pullulan tris(*n*-octadecylcarbamate) (PTODC).

Pullulan (1.0 g, 6.2 mmol per glucose unit) and LiCl (Tokyo Chemical Industry (TCI), Japan) (1.1 g, 24 mmol) were dried in a vacuum desiccator at 70 °C for at least 72 h over P_2O_5 (Fujifilm Wako Pure Chemical Co. (Fujifilm), Japan). The resulting pullulan and LiCl were added to *N*, *N*-dimethylacetamide (dehydrated grade, Fujifilm) (22 cm^3) at 95 °C under a nitrogen atmosphere and stirred with a magnetic bar for 12 h to completely dissolve the pullulan. Pyridine (dehydrated grade, Fujifilm) (25 cm^3) and an excess amount of *n*-butyl isocyanate (TCI) (5.5 g, 55 mmol) were added to the mixture and stirred to complete the reaction for 12 h. The resulting solution was poured into a large volume of water to precipitate the crude PTBC. The product was purified by successive fractional precipitation with methanol as solvent and water as precipitant.

Pullulan tris(ethylcarbamate) (PTEC) and pullulan tris(*n*-octadecylcarbamate) (PTODC) were also synthesized with ethyl isocyanate (TCI) and *n*-octadecyl isocyanate (TCI), respectively. Solubility tests were performed for PTEC, PTBC, and PTODC in common organic solvents. The solubility results are summarized in Table 1 along with literature data for amylose and cellulose tris(alkylcarbamate)s, amylose tris(ethylcarbamate) (ATEC) [39,40], amylose tris(*n*-butylcarbamate) (ATBC) [37,38,40], amylose tris(*n*-octadecylcarbamate) (ATODC) [40], cellulose tris(ethylcarbamate) (CTEC) [41], cellulose tris(*n*-butylcarbamate) (CTBC) [41], and cellulose tris(*n*-octadecylcarbamate) (CTODC) [41]. PTEC and PTBC exhibited solubilities comparable to the corresponding amylose and cellulose derivatives. In contrast, PTODC demonstrated a significantly lower solubility compared to ATODC and CTODC. As no suitable solvent could be identified for PTODC, subsequent solution characterization was performed only for PTEC and PTBC.

The chemical structures of PTBC and PTEC samples were confirmed by ^{1}H NMR (JNM-ECZ500 spectrometer, JEOL) in $CDCl_3$ and elemental analysis (CHN coder MT-6, YANACO). The results are summarized in Fig. S1 and Table S1 in the Supporting Information. The degree of substitution (DS) of the samples was calculated to be in the range of 3.1–3.5 from the weight ratio W_N/W_C of nitrogen to carbon, as summarized in Table 2, indicating complete substitution (DS = 3).

2.2. Size exclusion chromatography with multi angle light scattering (SEC-MALS)

SEC-MALS measurements were performed on the PTBC and PTEC samples using a DAWN DSP multi-angle light scattering photometer (Wyatt Technology Corporation, USA) with a He–Ne laser (wavelength λ_0 = 633 nm in a vacuum) and an RI-4030 refractive index detector (JASCO Corporation, Japan). A KF-G 4A guard column and a KF-806 M column (Shodex Co., Japan) were connected in series with the column temperature set at 40 °C. A sample loop of 100 μL was used, and the flow rate was set at 0.5 mL min^{-1}. The mass concentration *c* range of the injected solution was between 2.5 and 3.5 mg cm^{-3}. We have confirmed that the M_w value of a polystyrene standard sample, as evaluated by the instrument, matches the nominal value.

The specific refractive index increment $\partial n/\partial c$ values were measured using a modified Schulz-Cantow type differential refractometer (Shimadzu Co., Japan). The excess refractive index Δn was measured at three wavelengths (λ_0 = 436, 488, 546 nm) for three *c*. The $\partial n/\partial c$ value was determined for each λ_0 from the slope of the line (Fig. S2). The $\partial n/\partial c$ values in THF at 25 °C at λ_0 of the following light scattering instruments, were estimated from the linear relationship between $\partial n/\partial c$ and λ_0^{-2} (Fig. S3).

The excess scattering intensity and refractive index data were analyzed using square-root Zimm plot (Berry plot [43]) to estimate the weight-average molar mass M_w and the *z*-average radius of gyration $R_{g,z}$ as a function of the elution volume V_e (Fig. 2). The M_w values at high V_e

Table 1
Solubility of pullulan, amylose, and cellulose tris(alkylcarbamate)s in organic solvents at room temperature.

solvent	PTEC	ATEC[a]	CTEC[b]	PTBC	ATBC[c]	CTBC[b]	PTODC	ATODC[d]	CTODC[b]
chloroform	S	S	S	S	S	S	I	S	S
THF	S	S	S	S	S	S	I	S	S
MeOH	S	S	S	S	S	S	I	I	I
2-PrOH	S	S	I	S	S	S	I	I	I
1-PrOH	S	S	I	S	S	S	I	I	I
toluene	S	I		S	S		I	S	
acetone	S	S		S	S		I	I	
MTBE	I	I		S	S		I	S	

S: soluble. I: insoluble. MTBE: *tert*-butyl methyl ether.
[a] Ref. [39,40].
[b] Ref. [41].
[c] Ref. [37,38,40].
[d] Ref. [40].

Table 2
Molecular characteristics of PTBC and PTEC samples in THF at 25 °C.

sample	DS[a]	M_w[b]/kg mol^{-1}	$Đ$[b,c]	$R_{g,z}$/nm	A_2[d]/10^{-4} cm^3 mol g^{-2}	$[\eta]$ /cm^3 g^{-1}
PTBC780K	3.3	780	1.6	55.8[b]	N.D.[e]	219
PTBC300K	3.4	302	1.3	20.9[d]	2.5	96.3
PTBC130K	3.1	126	1.2	13.5[d]	3.2	49.2
PTEC840K	3.5	836	1.5	45.8[b]	N.D.[e]	141
PTEC320K	3.4	317	1.1	18.2[d]	2.4	74.8
PTEC210K	3.4	206	1.1	14.1[d]	2.4	52.5

[a] Elemental analysis.
[b] SEC-MALS.
[c] Defined as M_w/M_n.
[d] SAXS.
[e] Not determined.

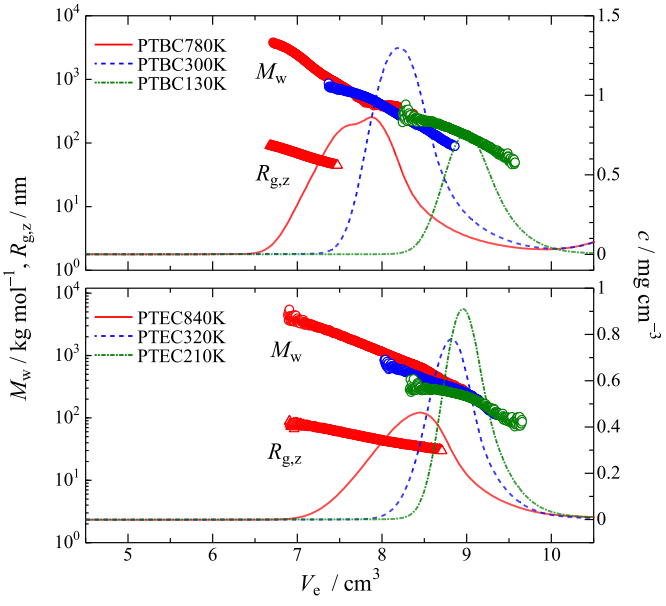

Fig. 2. Elution volume V_e dependence of the weight-average molar mass M_w (unfilled circles), the z-average mean-square radius of gyration $R_{g,z}$ (unfilled triangles), and the polymer mass concentration c (solid, dashed, and dot-dashed curves) for PTBC and PTEC in THF at 25 °C.

are not shown because they are less accurate due to low scattering intensity, as illustrated in Fig. S4. Additionally, only the $R_{g,z}$ values from the first half of the peak are shown in the figure since the data for the second half of the peak tend to be affected by high molar mass components. The obtained M_w, $R_{g,z}$, and the dispersity index $Đ$ ($\equiv M_w/M_n$ with M_n being the number-average molar mass) for each sample are shown in Table 2. It should be noted that the M_n and consequently the $Đ$ values can be affected by the SEC separation. As shown in Fig. 2 and Fig. S4, the M_w values are not completely consistent at the same V_e, most likely due to non-ideal SEC separation. Therefore, the M_n and $Đ$ values are considered less accurate than the M_w values.

2.3. Small-angle X-ray scattering (SAXS)

SAXS measurements were carried out for PTBC300K, PTBC130K, PTEC320K, and PTEC210K in THF at 25 °C at the BL40B2 beamline in SPring-8 (Hyogo, Japan). Test solutions with four different c ranging from 2.5 to 12.5 mg cm^{-3} were prepared for each sample and measured in a quartz glass capillary with a diameter of 2 mm. The wavelength λ_0, camera length (sample-to-detector distance), and accumulation time were set to 0.10 nm, 4.2 m, and 180 s, respectively. The scattered X-ray was detected using a Dectris Pilatus 3 2 M photon counter. The absolute value q of the scattering vector at each pixel of the detector was determined from the Bragg reflection of silver behenate placed at the sample cell. The scattering intensity $I(q)$ at q was obtained by circular averaging the two-dimensional data for the solutions at four different c and a solvent using exactly the same quartz capillary cell. The scattering intensities for the solution and solvent were compensated by the intensity detected downstream of the cell to evaluate the excess scattering intensity $\Delta I(q)$ as a function of q. The double logarithmic plots of $\Delta I(q)/c$ vs. q in Fig. S5 show almost no c dependence of $\Delta I(q)/c$ except in the low q range, suggesting good solubility as well as substantially no concentration dependence of the conformation of the polymer chains. A decreasing $\Delta I(q)/c$ with increasing c in the low q range is typical for linear polymers in good solvent systems. The square-root Zimm plot (Berry plot [43]) was therefore utilized for extrapolation to zero q and c to determine $R_{g,z}$, the second virial coefficients A_2, and the form factor $P(q)$. The resulting Berry plots are presented in Fig. S6, and the obtained $R_{g,z}$ and A_2 values for each sample are summarized in Table 2.

2.4. Viscometry

Solvent and solution viscosities for PTBC780K, PTBC300K, PTBC130K, PTEC840K, PTEC320K, and PTEC210K in THF at 25 °C were measured using a custom-made Ubbelohde-type viscometer, whose flow rate of THF was approximately 180 s. The intrinsic viscosity $[\eta]$ was determined from the Huggins and Mead-Fuoss plots as illustrated in Fig. S7. The resulting Huggins constant values were in the range of 0.25–0.36 for PTBC and 0.34–0.38 for PTEC, suggesting sufficient solubility of the samples in THF.

2.5. Infrared (IR) absorption

IR absorption measurements for PTBC300K and PTEC320K in THF at

25 °C (c = 15 mg cm^{-3}) were conducted using a FT/IR-4200 spectrometer (JASCO, Japan) with a CaF_2 solution cell with an optical path length of 0.05 mm.

3. Results and discussion

3.1. Dimensional and hydrodynamic properties in THF

Fig. 3 shows the molar mass dependence of $R_{g,z}$ for PTBC and PTEC in THF at 25 °C, together with data for amylose tris(alkylcarbamate) with the same side chain. The data points for PTBC and PTEC follow straight lines with $R^2_{g,z} = 1.0\ M_w^{1.1}$ and $R^2_{g,z} = 0.50\ M_w{}^{1.2}$, respectively, when the power-law relationship was applied to the current data as shown in Fig. S8. This is typical behavior of flexible polymers in good solvents. Both the data points and the slope for PTBC and PTEC are smaller than those for the corresponding amylose derivatives at the same M_w, indicating that the main chain of pullulan carbamates is more flexible than that of the corresponding amylose derivatives.

Fig. 4 illustrates the molar mass dependence of $[\eta]$ for PTBC and PTEC in THF at 25 °C, with the data for the corresponding amylose derivative. The data points are well described by straight lines, with $[\eta] = 3.1 \times 10^{-3} M_w^{0.82}$ for PTBC, and $[\eta] = 1.1 \times 10^{-2} M_w^{0.70}$ for PTEC as shown in Fig. S8, indicating that both PTBC and PTEC behave as typical semiflexible polymers in good solvents. As in the case of $R_{g,z}$, the smaller $[\eta]$ values and the weaker slope for the pullulan carbamates at the same M_w indicate a more flexible backbone.

To compare the current dimensional and hydrodynamic data for pullulan carbamates with literature data for pullulan in water [44–48], both $R_{g,z}$ and $[\eta]M_0$ are plotted against M_w/M_0 in Fig. 5, where M_0 is the molar mass of the repeating unit. Significantly higher values for both physical properties of pullulan carbamates clearly indicate the high chain stiffness, and the chain stiffness tends to be more significant with increasing side chain length.

The dimensional and hydrodynamic properties mentioned above indicate that both PTBC and PTEC behave as semiflexible chains in THF. In order to estimate the chain stiffness of semiflexible polymer chains in good solvent systems, intramolecular excluded volume effects should be considered with the quasi-two-parameter (QTP) theory [5,49,50]. Considering that the excluded volume effect becomes negligible with decreasing M_w, the form factor $P(q)$ for the low M_w samples is suitable to estimate the chain stiffness. The Holtzer plot (Fig. 6), where $qP(q)$ is plotted against q, for both PTBC and PTEC samples shows a mostly flat region in the middle and high q range, corresponding to the region where $P(q)$ is proportional to q^{-1}. This is known as the Holtzer plateau, where the absolute value is inversely proportional to the contour length L. On the other hand, the significant peak in the low q region indicates chain flexibility.

The experimental $P(q)$ data were analyzed in terms of the touched-bead wormlike chain model. The theoretical $P(q)$ can be written as [5,51,52].

$$P(q) = 9\left(\frac{2}{qd_b}\right)^6 \left(\sin\frac{qd_b}{2} - \frac{qd_b}{2}\cos\frac{qd_b}{2}\right)^2 P_0(q) \quad (1)$$

where d_b and $P_0(q)$ denote the diameter of the touched-bead (a measure of the chain thickness) and the form factor for the thin wormlike chain. $P_0(q)$ can be related to the characteristic function $I(L_K q; t/L_K)$ with the contour length L and the Kuhn segment length L_K as

$$P_0(q) = \frac{2}{L^2}\int_0^L (L-t) I(L_K q; t/L_K)\,dt \quad (2)$$

The numerical values for $I(L_K q; t/L_K)$ were calculated in terms of the Nakamura-Norisuye scheme [53,54] for the given L and L_K, where L_K is a measure of chain stiffness and twice the persistence length. Thus, theoretical $P(q)$ can be calculated with the three parameters of L, L_K, and d_b. A curve fitting procedure was employed for the data to determine the three parameters. The theoretical solid curves in Fig. 6 reproduce the experimental data almost quantitatively. The resulting values are summarized in Table 3, where the molar mass per unit contour length M_L ($\equiv M_w/L$) is given instead of L.

The radius of gyration R_g for perturbed wormlike chains can be calculated by combining QTP theory [5] and the Benoit-Doty equation [55] for the unperturbed wormlike chain. We chose the Domb-Barret function [56] for the relationship between the radius expansion factor α_s and the scaled excluded volume parameter $\tilde{z}$ [5]. In this scheme, R_g can be calculated as a function of molar mass from the three parameters, M_L, L_K, and the excluded volume strength B defined by β/a^2, where β and a denote the binary cluster integral representing the interaction between a pair of beads in a polymer chain and the bead spacing, respectively. However, the three parameters cannot be unambiguously determined due to the limited M_w range. Consequently, assuming that M_L and L_K are determined from $P(q)$, the experimental data can be well fitted by theoretical curves (Fig. 3) calculated with the B values listed in Table 3. The difference between the theoretical values with or without excluded volume effect is insignificant at the M_w's for the lower two M_w samples both for PTEC and PTBC, confirming the accuracy of the above-mentioned analysis for $P(q)$.

A similar analysis has been used for $[\eta]$. It is well known that the combination of the QTP theory [5] and the recent theory for the touched-bead unperturbed wormlike chain [5,57,58] can be used to calculate the theoretical $[\eta]$ with the parameters of M_L, L_K, d_b, and B.

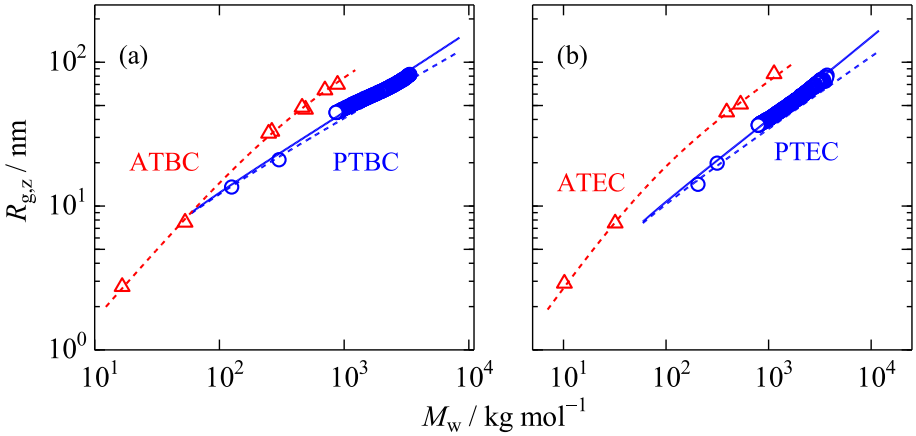

Fig. 3. M_w dependence of $R_{g,z}$ in THF at 25 °C for the pullulan alkylcarbamates. (a) PTBC (blue circles) and ATBC (red triangles) [37]. (b) PTEC (blue circles) and ATEC (red triangles) [39]. Solid and dashed curves represent theoretical values for the wormlike chains with and without excluded volume effects, respectively. (For interpretation of the references to colour in this figure legend, the reader is referred to the Web version of this article.)

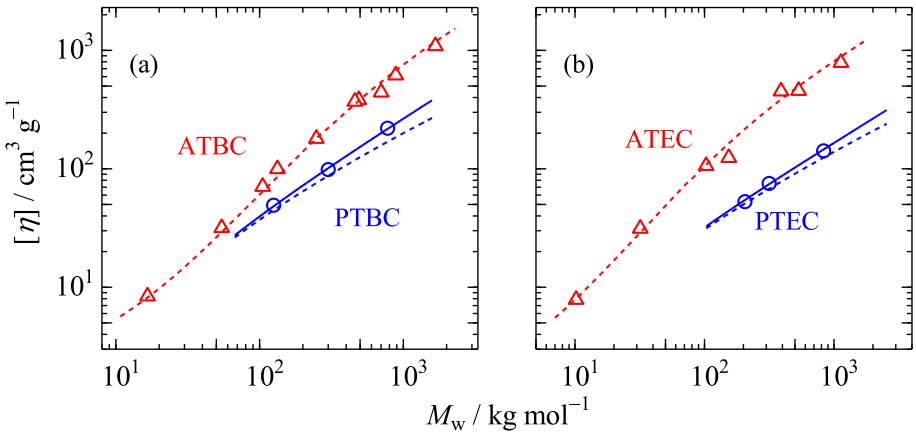

Fig. 4. M_w dependence of $[\eta]$ in THF at 25 °C for the pullulan alkylcarbamates. (a) PTBC (blue circles) and ATBC (red triangles) [37]. (b) PTEC (blue circles) and ATEC (red triangles) [39]. Solid and dashed curves represent theoretical values for the wormlike chains with and without excluded volume effects, respectively. (For interpretation of the references to colour in this figure legend, the reader is referred to the Web version of this article.)

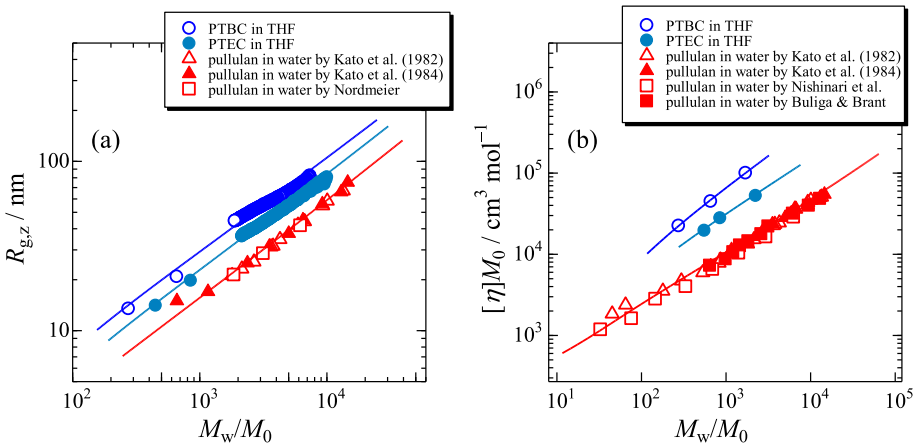

Fig. 5. M_w/M_0 dependence of (a) $R_{g,z}$ and (b) $[\eta]M_0$ for PTBC (unfilled circles) and PTEC (filled circles) in THF at 25 °C with the literature data for and pullulan in water at 25 °C [44–48].

Note that the Barret function [59] was utilized to calculate the viscosity expansion factor α_η^3 from $\tilde{z}$. As in the case of R_g, when we assumed M_L and L_K from $P(q)$, the remaining two parameters d_b and B were successfully determined from the curve fitting shown in Fig. 4. The resulting B from the two methods are in the same order. Considering that the two expansion factors are not significant even at the highest M_w, as found in Figs. 3 and 4 and furthermore, the molar mass dispersity could cause the experimental $R_{g,z}$, the small discrepancy in B may be acceptable. According to the QTP theory, A_2 can be calculated from L, L_K, and B. The calculated A_2 is quite close to the experimental values in Table 2. On the other hand, it should be noted that different d_b values from $P(q)$ and $[\eta]$ are reasonable because the former reflects the electron density profile of the chain contour and the latter can be influenced by the solvated molecules.

3.2. Comparison of wormlike chain parameters among pullulan alkylcarbamates, the other polysaccharide derivatives and native pullulan

The evaluated wormlike chain parameters for PTBC and PTEC are compared with pullulan [60] and the other polysaccharide butyl- and ethylcarbamates [37,39,41] in Table 4, where h is the contour length per monomer unit and is defined as M_0/M_L. Both PTBC and PTEC in THF have appreciably larger L_K values i.e., higher chain stiffness, than pullulan in aqueous media, suggesting that the side groups of PTBC and PTEC hinder the internal rotation of the main chain somewhat. This is reasonable, because significantly higher chain stiffness was observed for amylose carbamate derivatives in methanol [37,39] than amylose in dimethyl sulfoxide [61], where intramolecular hydrogen bonding was not substantially detected in the solution-state IR spectra. On the other hand, they are still much smaller than the previously investigated cellulose and amylose derivatives in THF. A prior study [62] on micro-Brownian motion suggested that the presence of α-1,6-glucosidic linkages in pullulan chains may cause large segmental mobility. SAXS measurements of oligo-pullulan in water also suggest that the presence of α-1,6-glucosidic linkages induces bending of the main chain [63]. Even after derivatization, the presence of the α-1,6-glucosidic linkage of the main chain allows a significant internal rotation compared to the main chain composed only of the α-1,4 and β-1,4-glucosidic linkages. This will be discussed in the next section in terms of the intramolecular hydrogen bonding of PTBC and PTEC. While the h value for PTEC is comparable to that of pullulan, a larger h value, but still shorter than the square root (0.479 nm) of the mean square length of the vector spanning each sugar residue [48,64], was evaluated for PTBC, suggesting that longer side groups extend the local conformation of the polysaccharide backbone. This side chain-dependent local conformational change has also been observed for cellulose and amylose derivatives [40,41].

3.3. Intramolecular hydrogen bonding and local conformation in THF

We have previously mentioned that the rigid helical structure

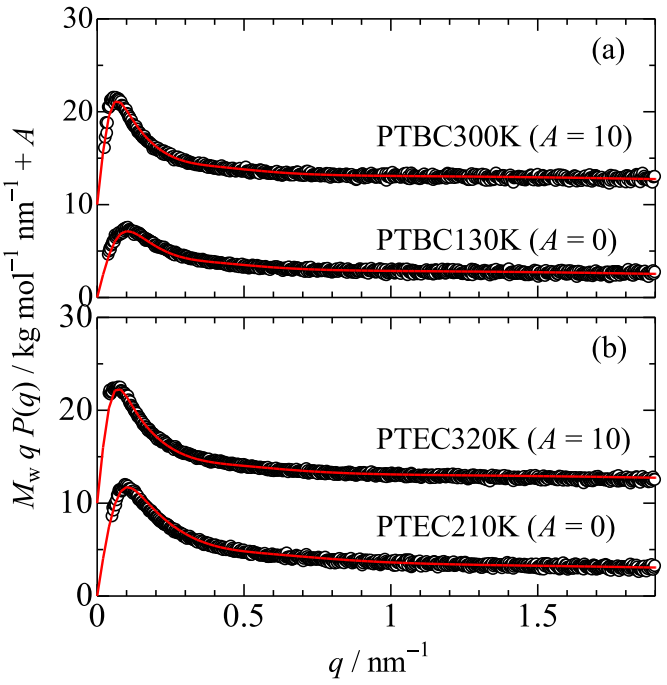

Fig. 6. Holtzer plots for PTBC and PTEC samples in THF at 25 °C. Solid red curves indicate theoretical values for the touched-bead wormlike chain with the parameters in Table 3. (For interpretation of the references to colour in this figure legend, the reader is referred to the Web version of this article.)

Table 3
Wormlike chain parameters for PTBC and PTEC in THF at 25 °C.

polymer	method	M_L/nm^{-1} kg mol^{-1}	L_K/nm	d_b/nm	B/nm
PTBC	$P(q)$	0.99 ± 0.063[a]	10.0 ± 1.0	1.0 ± 0.2	
	R_g	0.99	10.0		0.8 ± 0.2
	[η]	0.99	10.0	0.8 ± 0.2	1.3 ± 0.3
PTEC	$P(q)$	1.09 ± 0.040[a]	7.8 ± 0.5	1.0 ± 0.2	
	R_g	1.09	7.8		1.0 ± 0.2
	[η]	1.09	7.8	1.4 ± 0.3	0.5 ± 0.2

The ± symbol indicates that the parameter range reproduces the experimental values with consistent accuracy within that range.
[a] The mean values determined from either PTBC300K and PTBC130K or PTEC320K and PTEC210K. The parameters for each sample are shown in Table S2.

Table 4
Comparison of h and L_K values for polysaccharide tris(carbamate)s derivatives in THF at 25 °C and pullulan in water at 25 °C.

glucan chain	polymer	h/nm	L_K/nm	Ref.
α-1,4-; α-1,6-glucan	PTBC[a]	0.46 ± 0.03	10.0 ± 1.0	This work
α-1,4-; α-1,6-glucan	PTEC[a]	0.34 ± 0.01	7.8 ± 0.5	This work
α-1,4-glucan	ATBC[a]	0.26 ± 0.01	75 ± 5	[37]
α-1,4-glucan	ATEC[a]	0.36 ± 0.02	33 ± 3	[39]
β-1,4-glucan	CTBC[a]	0.40 ± 0.02	25 ± 1	[41]
β-1,4-glucan	CTEC[a]	0.45 ± 0.02	16.5 ± 1	[41]
α-1,4-; α-1,6-glucan	pullulan[b]	0.34	3.2	[60]

The ± symbol indicates that the parameter range reproduces the experimental values with consistent accuracy within that range.
[a] In THF at 25 °C.
[b] In water at 25 °C.

stabilized by the intramolecular hydrogen bonding plays an important role in the high chain stiffness of amylose alkylcarbamate in THF [37]. The intramolecular hydrogen bonding of polysaccharide carbamates can be observed from the amide I band of the infrared absorption spectra of the solution. This band reflects the hydrogen bonding structure of the carbonyl group on the carbamate groups [37,65]. Fig. 7 shows the wavenumber dependence of the molar absorption coefficients ε for PTBC300K and PTEC320K at 25 °C in THF. The figure includes literature data for amylose and cellulose tris(alkylcarbamate)s [37,39,41]. Only a single peak at 1737 cm^{-1} assigned to free carbonyl groups without hydrogen bonding, was found for both PTBC and PTEC; note that the small shoulder peak for PTBC and PTEC samples can be assigned to a small amount of weakly hydrogen-bonded carbonyl group. This is in contrast to the previously investigated amylose and cellulose derivatives for which another appreciable peak for hydrogen-bonded carbonyl group was found at 1698, 1700, 1714, and 1714 cm^{-1} for ATBC, ATEC, CTBC, and CTEC, respectively, with those for the free carbonyl group between 1737 and 1742 cm^{-1}. The difference in hydrogen bonding structure between pullulan and amylose derivatives clearly shows that a sufficient number of continuous α-1,4-glucosidic linkages are mandatory for the formation of intramolecular hydrogen bonds as well as the resulting rigid helical structure of amylose derivatives. As pointed out in our previous research, the local helical structure of amylose alkylcarbamates is determined by the packing structure of the alkyl chains inside the helical main chain [39]. Since only two continuous α-1,4-glucosidic linkages are not sufficient to form the helical structure, it can be confirmed that almost no hydrogen bonding is formed for PTBC and PTEC chains. This is consistent with the much smaller L_K values for the current pullulan derivatives than for the corresponding amylose carbamates shown in Table 4. In other words, not only the α-1,6-glucosidic linkages but also the α-1,4-glucosidic linkages have a low internal rotational barrier compared to the amylose derivatives with continuous α-1,4-glucosidic linkages as schematically illustrated in Fig. 8. This lower ability to form intramolecular hydrogen bonding may be a reason for the much lower solubility of PTODC as shown in Table 1.

4. Conclusions

Pullulan tris(ethylcarbamate) (PTEC) and pullulan tris(butylcarbamate) (PTBC) are well soluble in various organic solvents, including tetrahydrofuran (THF). Both the dimensional and hydrodynamic radii of PTEC and PTBC are much larger than those of pullulan at the same degree of polymerization, while they are smaller than those of the corresponding alkylcarbamate derivatives of amylose and cellulose. Analyses in terms of the wormlike chain with the excluded volume effect revealed that both PTEC and PTBC behave as semiflexible chains. The Kuhn segment length was determined to be 8 and 10 nm for PTEC and PTBC, respectively. The low chain stiffness is consistent with the low amount of intramolecular hydrogen bonding observed from the IR spectra. Comparison of the chain conformation between pullulan and amylose alkylcarbamates revealed that continuous α-1,4-glucosidic linkages are mandatory to form a rigid helical structure in solution. The significantly different hydrogen bonding structure of polysaccharide derivatives may play an important role in the molecular recognition ability of polysaccharide derivatives, including chiral separation.

CRediT authorship contribution statement

Yuki Matsumoto: Writing – review & editing, Writing – original draft, Investigation, Formal analysis, Data curation. **Shinichi Kitamura:** Writing – review & editing, Supervision, Resources. **Rintaro Takahashi:** Writing – review & editing. **Ken Terao:** Writing – review & editing, Writing – original draft, Supervision, Funding acquisition, Conceptualization.

Declaration of competing interest

The authors declare the following financial interests/personal relationships which may be considered as potential competing interests: Ken Terao reports financial support was provided by Japan Society for

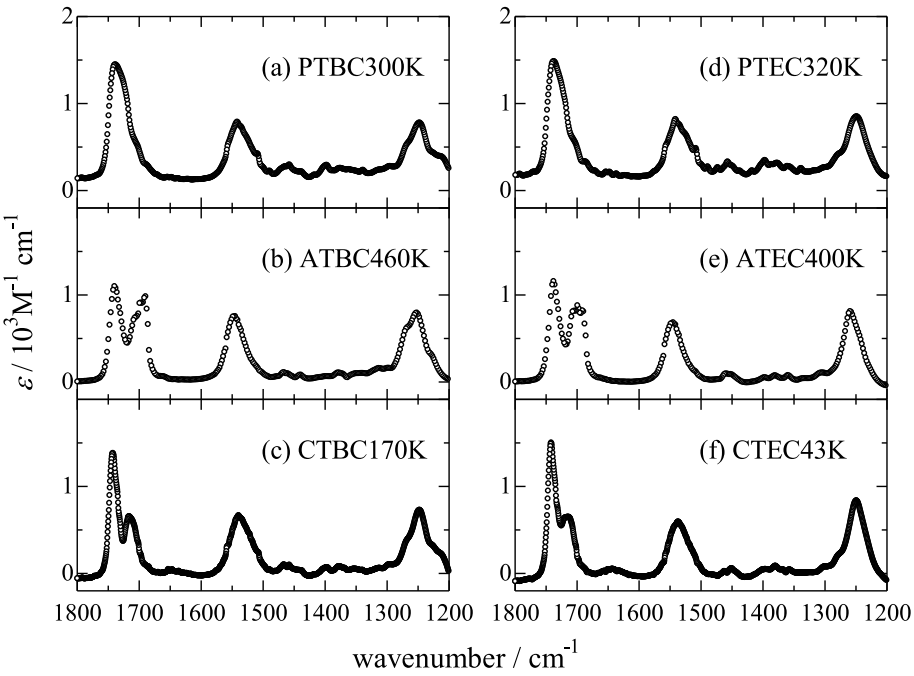

Fig. 7. IR spectra (molar absorption coefficient ε vs wavenumber) for polysaccharide tris(alkylcarbamate)s in THF at 25 °C.

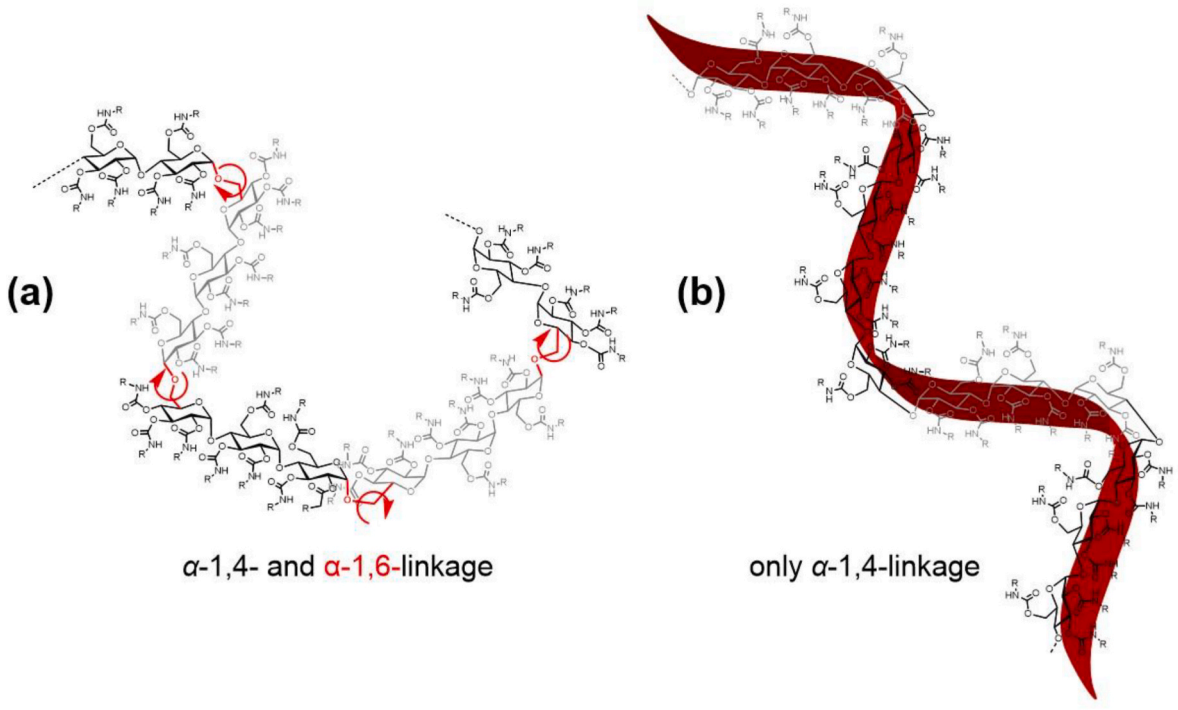

Fig. 8. Schematic representation of the linkages and conformational feature of (a) pullulan tris(alkylcarbamate)s and (b) amylose tris(alkylcarbamate)s in THF.

the Promotion of Science. If there are other authors, they declare that they have no known competing financial interests or personal relationships that could have appeared to influence the work reported in this paper.

Acknowledgments

The authors are grateful to Dr. Noboru Ohta (SPring-8) for the SAXS measurements. The synchrotron radiation experiments were performed at the BL40B2 in SPring-8 with the approval of the Japan Synchrotron Radiation Research Institute (JASRI) (Proposal Nos. 2023A1111, 2023A1112, and 2024A1209). This work was the result of the use of research equipment (NMR, IR, and ultimate analysis) shared under the MEXT Project for promoting public utilization of advanced research infrastructure (Program for supporting construction of core facilities) Grant No. JPMXS0441200022 and JPMXS0441200023. This work was partially supported by Japan Society for the Promotion of Science (JSPS) KAKENHI grant No. JP23K26704.

Appendix A. Supplementary data

Supplementary data to this article can be found online at https://doi.org/10.1016/j.polymer.2025.128417.

Data availability

Data will be made available on request.

References

[1] P.J. Flory, Principles of Polymer Chemistry, Cornell University Press, Ithaca, N. Y., 1953.
[2] P.J. Flory, Statistical Mechanics of Chain Molecule, Interscience, New York, 1969.
[3] Y. Sasanuma, Conformational Analysis of Polymers: Methods and Techniques for Structure-Property Relationships and Molecular Design, Wiley, 2023.
[4] O. Kratky, G. Porod, Rontgenuntersuchung geloster fadenmolekule, recueil des travaux chimiques des pays-bas, J. R. Netherlands Chem. Soc. 68 (1949) 1106–1122.
[5] H. Yamakawa, T. Yoshizaki, Helical Wormlike Chains in Polymer Solutions, second ed., Springer, Berlin, Germany, 2016.
[6] W. Burchard, Light scattering from polysaccharides as soft materials, in: R. Borsali, R. Pecora (Eds.), Soft Matter Characterization, Springer, Netherlands, 2008, pp. 463–603.
[7] W. Burchard, Uber Die Gestalt Von Amylose- und Cellulosetricarbanilat in Verschiedenen Losungsmitteln, Zeitschrift Fur Physikalische Chemie-Frankfurt 42 (1964) 293–313.
[8] W. Burchard, Uber Die Abweichungen Von Der Idealen Knauelstatistik Bei Amylose- Und Cellulosetricarbanilat in Einem Theta-Losungsmittel, Makromol. Chem. 88 (1965) 11–28.
[9] W. Burchard, Statistics of stiff chain molecules. III. Chain length dependence of the mean square radius of gyration of cellulose and amylose-tricarbanilates, Br. Polym. J. 3 (1971) 214–221.
[10] W. Sutter, W. Burchard, Comparative-study of hydrodynamic properties of cellulose and amylose tricarbanilates in dilute-solutions - Viscosity, sedimentation and diffusion measurements in 1,4-Dioxane in molecular-weight range of $500 < M < 5 . 10^6$, Makromol. Chem. 179 (1978) 1961–1980.
[11] A.K. Gupta, E. Marchal, W. Burchard, H. Benoit, Persistence length of cellulose tricarbanilate by small-angle neutron-scattering, Polymer 17 (1976) 363–366.
[12] J.M.G. Cowie, Studies on amylose and its derivatives .6. estimation of cohesive energy densities of some amylose derivatives, Biopolymers 3 (1965) 69–78.
[13] W. Banks, C.T. Greenwood, J. Sloss, The hydrodynamic behaviour of amylose tricarbanilate in dilute solution. III. The relations between viscosity, sedimentation coefficient, molecular weight, and coil dimensions for amylose tricarbanilate in a pyridine/water theta-solvent, Makromol. Chem. 140 (1970) 109–118.
[14] W. Banks, C.T. Greenwood, J. Sloss, The hydrodynamic behaviour of amylose tricarbanilate in dilute solution. IV. A comparison of experimental and calculated coil dimensions for amylose tricarbanilate in a pyridine/water theta-solvent, Makromol. Chem. 140 (1970) 119–129.
[15] W. Banks, C.T. Greenwood, The hydrodynamic behaviour of amylose tricarbanilate in dilute solution. V. The estimation of the unperturbed dimensions of amylose tricarbanilate from measurements carried out in good solvents, Makromol. Chem. 144 (1971) 135–153.
[16] W. Banks, C.T. Greenwood, J. Sloss, Physicochemical studies on starches .52. Hydrodynamic behaviour of amylose tricarbanilate in dilute solution .2. comparison of experimental and calculated coil dimensions for amylose tricarbanilate in pyridine, Eur. Polym. J. 7 (1971) 879–888.
[17] B. Pfannemuller, M. Schmidt, G. Ziegast, K. Matsuo, Properties of a once-broken wormlike chain based on amylose tricarbanilate - light-scattering, viscosity, and dielectric-relaxation, Macromolecules 17 (1984) 710–716.
[18] Y. Muroga, K. Hayashi, M. Fukunaga, T. Kato, S. Shimizu, K. Kurita, Change of the persistence lengths in the conformational transitions of pullulan- and amylose-tricarbanilates, Biophys. Chem. 121 (2006) 96–104.
[19] F. Kasabo, T. Kanematsu, T. Nakagawa, T. Sato, A. Teramoto, Solution properties of cellulose tris(phenyl carbamate). 1. Characterization of the conformation and intermolecular interaction, Macromolecules 33 (2000) 2748–2756.
[20] A. Tsuboi, M. Yamasaki, T. Norisuye, A. Teramoto, Dilute-solution behavior of cellulose Tris(3,5-dimethylphenylcarbamate), Polym. J. 27 (1995) 1219–1229.
[21] A. Tsuboi, T. Norisuye, A. Teramoto, Chain stiffness and excluded-volume effects in dilute polymer solutions: cellulose tris (3,5-dimethylphenyl)carbamate, Macromolecules 29 (1996) 3597–3602.
[22] H. Yanai, T. Sato, Local conformation of the cellulosic chain in solution, Polym. J. 38 (2006) 226–233.
[23] H. Bittiger, G. Keilich, Optical rotatory dispersion and circular dichroism of carbanilyl polysaccharides, Biopolymers 7 (1969) 539–556.
[24] K. Terao, T. Fujii, M. Tsuda, S. Kitamura, T. Norisuye, Solution properties of amylose tris(phenylcarbamate): local conformation and chain stiffness in 1,4-Dioxane and 2-Ethoxyethanol, Polym. J. 41 (2009) 201–207.
[25] Y. Okamoto, E. Yashima, Polysaccharide derivatives for chromatographic separation of enantiomers, Angew Chem. Int. Ed. Engl. 37 (1998) 1020–1043.
[26] E. Yashima, Polysaccharide-based chiral stationary phases for high-performance liquid chromatographic enantioseparation, J. Chromatogr. A 906 (2001) 105–125.
[27] T. Ikai, Y. Okamoto, Structure control of polysaccharide derivatives for efficient separation of enantiomers by chromatography, Chem. Rev. 109 (2009) 6077–6101.
[28] M. Lammerhofer, Chiral recognition by enantioselective liquid chromatography: mechanisms and modern chiral stationary phases, J. Chromatogr. A 1217 (2010) 814–856.
[29] G.K.E. Scriba, Chiral recognition in separation sciences. Part I: polysaccharide and cyclodextrin selectors, TrAC, Trends Anal. Chem. 120 (2019) 115639.
[30] G. Félix, T. Zhang, An amylopectin tris(phenylcarbamate) chiral stationary phase for high performance liquid chromatography, J. High Resolut. Chromatogr. 16 (1993) 364–367.
[31] G. Félix, T. Zhang, Chiral packing materials for high-performance liquid chromatographic resolution of enantiomers based on substituted branched polysaccharides coated on silica gel, J. Chromatogr. A 639 (1993) 141–149.
[32] P. Wang, D. Liu, S. Jiang, X. Gu, Z. Zhou, The direct chiral separations of fungicide enantiomers on amylopectin based chiral stationary phase by HPLC, Chirality 19 (2007) 114–119.
[33] A. Ryoki, Y. Kimura, S. Kitamura, K. Maeda, K. Terao, Does local chain conformation affect the chiral recognition ability of an amylose derivative? Comparison between linear and cyclic amylose tris(3,5-dimethylphenylcarbamate), J. Chromatogr. A 1599 (2019) 144–151.
[34] A. Kishimoto, M. Mizuguchi, A. Ryoki, K. Terao, Molecular structure and chiral recognition ability of highly branched cyclic dextrin carbamate derivative, Carbohydr. Polym. 290 (2022) 119491.
[35] A. Kishimoto, A. Ryoki, S. Kitamura, K. Terao, Correlation between conformational feature in solution and chiral separation ability of linear and nonlinear amylose tris (alkylcarbamate)s, Polymer 284 (2023) 126303.
[36] K. Terao, T. Sato, Conformational properties of polysaccharide derivatives, in: G. Yang, L. Lamboni (Eds.), Bioinspired Materials Science and Engineering, 2018, pp. 167–183.
[37] K. Terao, M. Murashima, Y. Sano, S. Arakawa, S. Kitamura, T. Norisuye, Conformational, dimensional, and hydrodynamic properties of amylose tris(*n*-Butylcarbamate) in tetrahydrofuran, methanol, and their mixtures, Macromolecules 43 (2010) 1061–1068.
[38] Y. Sano, K. Terao, S. Arakawa, M. Ohtoh, S. Kitamura, T. Norisuye, Solution properties of amylose tris(n-butylcarbamate). Helical and global conformation in alcohols, Polymer 51 (2010) 4243–4248.
[39] K. Terao, F. Maeda, K. Oyamada, T. Ochiai, S. Kitamura, T. Sato, Side-chain-dependent helical conformation of amylose alkylcarbamates: amylose tris (ethylcarbamate) and amylose tris(n-hexylcarbamate), J. Phys. Chem. B 116 (2012) 12714–12720.
[40] A. Ryoki, D. Kim, S. Kitamura, K. Terao, Linear and cyclic amylose derivatives having brush like side groups in solution: amylose tris(n-octadecylcarbamate)s, Polymer 137 (2018) 13–21.
[41] X.Y. Jiang, A. Ryoki, K. Terao, Dimensional and hydrodynamic properties of cellulose (alkylcarbamate)s in solution: side chain dependent conformation in tetrahydrofuran, Polymer 112 (2017) 152–158.
[42] K. Terao, A. Ryoki, S. Kitamura, T. Sato, Molecular conformation and intermolecular interactions of linear and cyclic amylose derivatives in solution, Macromol. Symp. 408 (2023) 2200024.
[43] G.C. Berry, T.A. Orofino, Branched polymers. III. Dimensions of chains with small excluded volume, J. Chem. Phys. 40 (1964) 1614–1621.
[44] T. Kato, T. Okamoto, T. Tokuya, A. Takahashi, Solution properties and chain flexibility of pullulan in aqueous-solution, Biopolymers 21 (1982) 1623–1633.
[45] T. Kato, T. Katsuki, A. Takahashi, Static and dynamic properties of pullulan in a dilute-solution, Macromolecules 17 (1984) 1726–1730.
[46] E. Nordmeier, Static and dynamic light-scattering solution behavior of pullulan and dextran in comparison, J. Phys. Chem. 97 (1993) 5770–5785.
[47] K. Nishinari, K. Kohyama, P.A. Williams, G.O. Phillips, W. Burchard, K. Ogino, Solution properties of pullulan, Macromolecules 24 (1991) 5590–5593.
[48] G.S. Buliga, D.A. Brant, Temperature and molecular weight dependence of the unperturbed dimensions of aqueous pullulan, Int. J. Biol. Macromol. 9 (1987) 71–76.
[49] H. Yamakawa, W.H. Stockmayer, Statistical mechanics of wormlike chains. II. Excluded volume effects, J. Chem. Phys. 57 (1972) 2843–2854.
[50] J. Shimada, H. Yamakawa, Statistical-mechanics of helical worm-like chains .25. excluded-volume effects, J. Chem. Phys. 85 (1986) 591–600.
[51] W. Burchard, K. Kajiwara, The statistics of stiff chain molecules I. The particle scattering factor, Proc. Roy. Soc. Lond. Math. Phys. Sci. 316 (1970) 185–199.
[52] K. Nagasaka, T. Yoshizaki, J. Shimada, H. Yamakawa, More on the scattering function of helical wormlike chains, Macromolecules 24 (1991) 924–931.
[53] Y. Nakamura, T. Norisuye, Brush-like polymers, in: R. Borsali, R. Pecora (Eds.), Soft Matter Characterization, Springer Netherlands, 2008, pp. 235–286.
[54] Y. Nakamura, T. Norisuye, Scattering function for wormlike chains with finite thickness, J. Polym. Sci., Part B: Polym. Phys. 42 (2004) 1398–1407.
[55] H. Benoit, P. Doty, Light scattering from non-gaussian chains, J. Phys. Chem. 57 (1953) 958–963.
[56] C. Domb, A.J. Barrett, Universality approach to expansion factor of a polymer-chain, Polymer 17 (1976) 179–184.
[57] H. Yamakawa, M. Fujii, Intrinsic viscosity of wormlike chains. Determination of the shift factor, Macromolecules 7 (1974) 128–135.
[58] H. Yamakawa, T. Yoshizaki, Transport coefficients of helical wormlike chains. 3. Intrinsic viscosity, Macromolecules 13 (1980) 633–643.
[59] A.J. Barrett, Intrinsic viscosity and friction coefficients for an excluded volume polymer in the kirkwood approximations, Macromolecules 17 (1984) 1566–1572.
[60] J. Yang, T. Sato, Conformation of pullulan in aqueous solution studied by small-angle X-Ray scattering, Polymers (Basel) 12 (2020) 1266.

[61] Y. Nakanishi, T. Norisuye, A. Teramoto, S. Kitamura, Conformation of amylose in dimethyl-sulfoxide, Macromolecules 26 (1993) 4220–4225.
[62] S. Kitamura, H. Tanahashi, T. Kuge, Study of polysaccharides by the fluorescence method. III. Chain length dependence of the micro-brownian motion of amylose in an aqueous solution, Biopolymers 23 (2004) 1043–1056.
[63] J.H.Y. Liu, D.A. Brant, S. Kitamura, K. Kajiwara, R. Mimura, Equilibrium spatial distribution of aqueous pullulan: small-Angle X-ray scattering and realistic computer modeling, Macromolecules 32 (1999) 8611–8620.
[64] B.A. Burton, D.A. Brant, Comparative flexibility, extension, and conformation of some simple polysaccharide chains, Biopolymers 22 (1983) 1769–1792.
[65] R.B. Kasat, Y. Zvinevich, H.W. Hillhouse, K.T. Thomson, N.H. Wang, E.I. Franses, Direct probing of sorbent-solvent interactions for amylose tris(3,5-dimethylphenylcarbamate) using infrared spectroscopy, X-ray diffraction, solid-state NMR, and DFT modeling, J. Phys. Chem. B 110 (2006) 14114–14122.